Applied Catalysis B: Environmental 108–109 (2011) 168–176

Contents lists available at SciVerse ScienceDirect

Applied Catalysis B: Environmental

journal homepage: www.elsevier.com/locate/apcatb

Solar light assisted photodegradation of phenol with hydrogen peroxide over iron-doped titania catalysts: Role of iron leached/readsorbed species

C. Adán[a], J. Carbajo[a], A. Bahamonde[a], I. Oller[b], S. Malato[b], A. Martínez-Arias[a,*]

[a] Instituto de Catálisis y Petroleoquímica, ICP-CSIC. C/ Marie Curie 2, Cantoblanco, 28049 Madrid, Spain
[b] Plataforma Solar de Almería-CIEMAT, Ctra. de Senés s/n, 04200 Tabernas, Almería, Spain

ARTICLE INFO

Article history:
Received 29 June 2011
Received in revised form 29 July 2011
Accepted 18 August 2011
Available online 24 August 2011

Keywords:
Solar light
Photocatalysis
Iron leaching
Phenol photooxidation
TiO_2
H_2O_2

ABSTRACT

Nanostructured iron-doped TiO_2 catalysts with anatase structure and two different iron contents (0.7 and 3.5 wt.%) have been prepared by a combined sol–gel/microemulsion method and examined with respect to their behaviour for photocatalytic degradation of aqueous phenol with H_2O_2 under solar light. The activity results are compared with those obtained for similarly prepared undoped systems as well as Degussa P25 reference catalyst and have been complemented with structural/morphological and electronic characterization analyses achieved by XRD, TEM, Raman, S_{BET}, UV–vis DRS and XPS techniques. In contrast to typically observed results, the highest photoactivity is obtained for the catalyst with highest iron loading while that with 0.7% Fe displays lower photoactivity than undoped samples. Such unusual behaviour has been attributed to the contribution of new photoactive iron complexes generated on the surface of the catalyst as a consequence of iron leaching and readsorption processes taking place during the course of phenol photodegradation process.

1. Introduction

Phenolic compounds constitute an important family of pollutants of wastewater produced by chemical, petrochemical, food-processing or biotechnological industries. Current levels of pollutants removal from water, achievable upon employment of conventional water treatment technologies, are often not fully satisfactory when waste water streams contain significant amounts of hardly biodegradable chemicals or compounds having phytotoxic effect on the microorganism responsible for biological degradation of the organic waste, as phenolic type pollutants [1]. Among possible technologies to accomplish this task, novel and economically interesting oxidation techniques based on catalytic or chemical photooxidation processes are emerging as a promising alternative [2–5].

Heterogeneous photocatalytic oxidation employing semiconductors excitable by solar light appears most attractive in this sense. Semiconductor photocatalysis has been the focus of numerous investigations because of its application to the quantitative destruction of undesirable chemical contaminants in water and air [2,4,6,7]. Polycrystalline titanium dioxide presents unique properties for this purpose since it is a stable material able to mineralize refractory organic pollutants present in effluent water under ambient pressure and temperature condition [2,4,5,7–10]. However, its photocatalytic efficiency can be limited by stabilization of the charge photocarriers in the bulk of the material, by fast electron–hole recombination either at the bulk or at the surface of the oxide or by its relatively large band gap which limits light absorption in the visible region [2,4,6–8].

Among strategies aimed at reducing electron–hole recombination rates and to decrease simultaneously the band gap of the material, it is common to employ methods based on doping the titania catalyst with transition metal cations while maintaining a good control of the primary particle size to achieve nanoscale configurations of the catalysts [8,11–13]. Fe^{3+} is considered an interesting dopant of titania although its catalytic role during photooxidation processes is controversial [10,14–17]. It is believed that Fe^{3+} cations can act as shallow traps in the titania lattice although discrepancies appear with respect to their role concerning electron/hole recombination properties [7,15]. In general terms, it appears that optimum photocatalytic properties can be achieved upon doping at a relatively weak level [10,15], which can be closely related to the dynamics of the recombination process, in turn linked to the distance between dopant cations in the titania lattice [15]. Additionally, modifications of the surface properties induced by doping as well as the possibility that iron lixiviates formed upon interaction with carboxylic acids participate in the reaction mechanism can be of relevancy to explain the photocatalytic performance of this type of photocatalysts [10,18,19]. The photochemical or photocatalytic oxidation of phenol using UV or visible light employing

* Corresponding author. Tel.: +34 915 85 49 40; fax: +34 915 85 47 60.
E-mail address: amartinez@icp.csic.es (A. Martínez-Arias).

0926-3373/$ – see front matter © 2011 Elsevier B.V. All rights reserved.
doi:10.1016/j.apcatb.2011.08.026

TiO_2 or Fe-doped TiO_2 as catalyst and hydrogen peroxide as oxidant under laboratory conditions have been examined in previous works [20,21]. It is generally concluded that the use of H_2O_2 as oxidizing agent can significantly enhance the phenol oxidation rate and that the number and amount of intermediates formed can be decreased under heterogeneous conditions, i.e. in the presence of the solid photocatalyst [20,21]. However, experimental conditions must be carefully selected since hydrogen peroxide can also act as hydroxyl radical scavenger limiting the photoefficiency of the system for pollutant removal [21].

Within this context, the present work aims to explore the photoactivity of nanostructured iron-doped titania catalysts for phenol photooxidation with H_2O_2 under solar light irradiation in pilot plant conditions. Information achieved by employing different structural and electronic characterization techniques (XRD, TEM, Raman, S_{BET}, as well as UV–vis and XPS spectroscopies) has been employed to complement the results of catalytic testing for the phenol mineralization reaction. The results indicate an important role for leached/readsorbed iron species, which apparently allows overcoming intrinsic difficulties of the doped catalyst for the process.

2. Experimental

Iron-doped photocatalysts were prepared using a combined sol–gel/microemulsion preparation method. Titanium-tetraisopropoxide was added to a reverse microemulsion in which the aqueous phase contains a solution of iron (III) nitrate nonahydrate; this was dispersed in *n*-heptane, using Triton X-100 (Aldrich) as surfactant and 1-hexanol as cosurfactant; further details of the procedure employed can be found elsewhere [10]. The resulting mixture was stirred for 24 h, centrifuged, decanted, rinsed with methanol and dried at room temperature for 12 h. Then, the amorphous mixed oxide was calcined for 2 h at 450 °C under air atmosphere. Nominal iron amounts employed (0.7 and 3.5 wt.% corresponding to ca. 1 and 5 at.%) were similar (within experimental error) to experimental contents determined by ICP-OES. A reference undoped TiO_2 catalyst was prepared by using the same method. The catalysts will be referred to hereafter as 450-T0, 450-T1 and 450-T5, the nomenclature reflecting the calcination temperature employed for the preparation and the iron at.% loading of the catalysts. A commercial titania Degussa P25 catalyst was also employed as a reference.

Powder XRD patterns were obtained with a Siemens D-500 apparatus using nickel-filtered Cu Kα radiation operating at 40 kV and 40 mA, with a 0.04° step size and accumulating a total of 5 s per point; crystal size (estimated by using the Scherrer equation) and lattice parameter determinations were made from XRD (1 0 1) and (2 0 0) anatase peaks appearing, respectively, at ca. 25.8° and 48.8° (2θ) using the Analyze RayfleX 2.293 program for fitting and analysis. High resolution transmission electron microscopy (TEM) images were obtained with a JEOL JEM 2100 F UHR electron microscope. Specimens were prepared by depositing particles of the catalysts from acetone dispersions onto a copper grid supporting a perforated carbon film. Raman data were acquired using a Renishaw dispersive system 1000, equipped with a single monochromator, a holographic notch filter, and a cooled TCD; the catalysts were excited using the 514 nm emission line of an Ar laser. The diffuse reflectance absorption spectra of the photocatalysts were recorded with a UV–vis Varian 2300 apparatus. Nitrogen adsorption–desorption isotherms and the specific surface areas were examined by the BET method and measured at liquid nitrogen temperature with a Micromeritics Tristar automatic apparatus on catalysts previously outgassed overnight at 180 °C to a vacuum of $<10^{-4}$ Pa to ensure a dry clean surface free from any loosely held adsorbed species. X-ray photoelectron spectroscopy (XPS) studies were performed with a VG Escalab 200R spectrometer employing a Mg Kα (1253.6 eV) X-ray source. The catalyst was first placed in a copper holder mounted on a sample-rod in the pre-treatment chamber of the spectrometer and then outgassed at room temperature for 1 h before being transferred to the analysis chamber. The desired region of the spectrum was then scanned a number of times in order to obtain a good signal to noise ratio. The binding energies (BE) were referenced to the spurious C1s peak (284.6 eV) used as an internal standard to take into account charging effects. The areas of the peaks were computed by fitting the experimental spectra to Gaussian/Lorentzian curves after removal of the background (Shirley function). Surface atom ratios were calculated from peak area ratios normalized by the appropriate atomic sensitivity factors [22].

Photoreactors based on compound parabolic collectors (CPCs) from the Plataforma Solar de Almería (PSA) were employed to study the solar light photodegradation of phenol. The static collectors present a reflective aluminium surface with an absorber tube in the focus, which provide highly efficient light-harvesting optics for low concentration systems [23]. One advantage of CPC reactors is that the whole solar radiation reaching the collectors (both direct and diffuse) can be potentially collected by the reflector mirrors [23]. Waste water circulates under turbulent flow conditions inside the CPC absorber tubes within a closed recirculating system. The hydraulic circuit of the photoreactor is formed by a continuously stirred tank, a re-circulation pump and a solar collector which consists in three CPC modules arranged in series and placed on fixed supports inclined 37° (latitude of PSA) with respect to the horizontal plane. The plant is designed for operation in batch mode. The total volume in the experiments was 35 L and the volume irradiated in the solar collector was 22 L. A detailed description of the characteristics of the materials and components used in this set-up is given elsewhere [24]. The starting conditions were the following: 50 mg L^{-1} of phenol, 500 mg L^{-1} of H_2O_2 and 200 mg L^{-1} of catalyst, added to the 35 L stirred tank; an initial pH value of ca. 6.5 was obtained under these conditions in the reactant dispersion. Evaluation of weather conditions, required to normalize the intensity of the solar irradiance for experiments done during different days, was done by means of a Kipp&Zonen CUV3 broadband UV radiometer with UV range (285–400 nm). It was inclined 37° (local latitude in PSA) and oriented to the equator like the CPC photoreactor. A normalized illumination time, defined elsewhere [24], was selected to normalize the solar irradiation. In this approach, the average solar UV flux on a perfect sunny day is considered as 30 W_{UV} m^{-2}; accordingly, the irradiation time will be represented as $t_{30\,W}$.

The total organic content (TOC) of aqueous samples was determined with a Shimadzu TOC-5050A analyzer equipped with a Shimadzu ASI-5000A autosampler. Phenol or aromatic intermediates concentrations were monitored by high performance liquid chromatography with UV detection (HPLC-UV), employing a nucleosil C-18 column at 50 °C and water/methanol at 65/35 ratio as mobile phase. The concentrations of short-chain organic acids formed during the photocatalytic process were measured with a Dionex DX-600 chromatograph, using a Dionex Ionpac AS11-HC 4 × 250 mm anion column with a mobile phase of H_2O/NaOH 100 mM. The H_2O_2 content was measured by iodometric titration using KI 0.2 M, $Na_2S_2O_3$ 0.05 M and a starch indicator. Measurements of iron (II) and total iron lixiviates to the reaction medium were made by the orthophenanthroline method by means of a UV–vis Unicam-III spectrophotometer at 510 nm (maximum wave length of the iron–phenanthroline complex) with an estimated detection limit under employed conditions of 0.1 ppm; note this method can be used to measure iron (II) and total iron contents by the addition of a little amount of ascorbic acid ($C_6H_8O_6$, Sigma

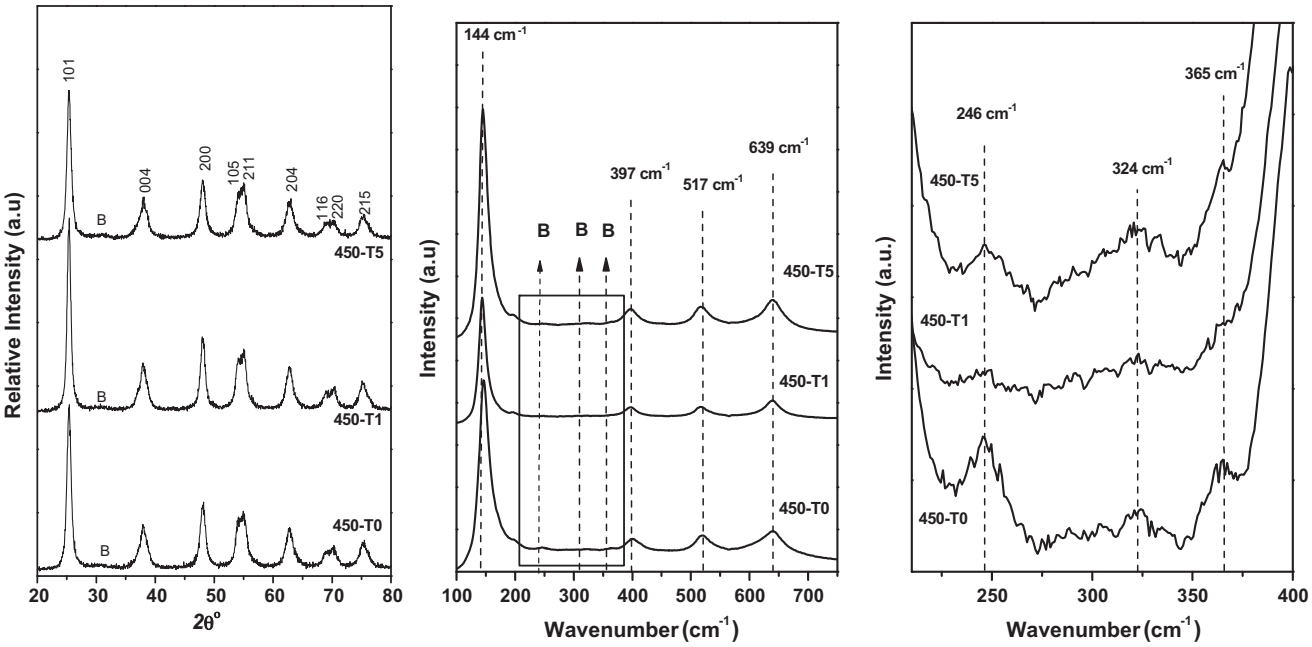

Fig. 1. Left: X-ray diffractograms of the indicated catalysts. Miller indexes of most intense peaks of the anatase phase are indicated. Label B corresponds to most intense peak of the brookite phase of titania. Middle: Raman spectra of the indicated samples. Peaks attributed to the brookite phase of titania are marked as B. A detail of the Raman spectra in the zone in which main brookite peaks are detected (see text) is shown in the right plot.

ultra), while the amount of iron (III) is estimated by subtracting between total iron and iron (II) amounts.

3. Results and discussion

3.1. Characterization of the catalysts

X-ray diffractograms and Raman spectra of the catalysts are displayed in Fig. 1. Table 1 summarizes main structural parameters derived from analysis of such results and whose details can be found elsewhere [10]. In brief, the catalysts are basically constituted by the anatase form of titania. Residual amounts of the brookite phase of titania are evidenced upon perusal of the Raman spectra; such phase is proposed to be responsible of the broad poorly resolved feature in the X-ray diffractogram detected for these catalysts between $2\theta = 25$ and 35°, at which most intense peaks of brookite titania are expected [25]. Further details on morphological characteristics of the catalysts have been obtained by TEM. As shown in Fig. 2, the catalysts are generally constituted by polyhedral more or less spherical crystals (within aggregates in the micron size), displaying average crystal sizes in qualitative agreement with XRD results (Table 1).

No hint of iron containing phases was obtained from XRD, TEM or Raman results, which reveals a relatively high degree of dispersion for this component in any of the cases. Some details on the state of iron can be achieved from analysis of UV–vis spectra (Fig. 3). Thus, the undoped catalyst displays a steep increase of the absorption at wavelength lower than 380 nm (ca. 3.2 eV), attributed to the intrinsic band gap absorption of pure anatase TiO_2. The presence of iron produces a new contribution in the visible region below ca. 400 nm, which increases with the iron content; this is in consistency with changes observed in the colour of the catalysts from white, for the undoped catalyst, to yellow or finally light brown as the iron loading increases. Apparently two components at about 400 and 500 nm, respectively, contribute to this enhanced absorption in the visible region, as detailed in a previous work [10]. To summarize, the band at ca. 400 nm can be attributed to more or less isolated Fe^{3+} cations while the band at ca. 500 nm can be related to the presence

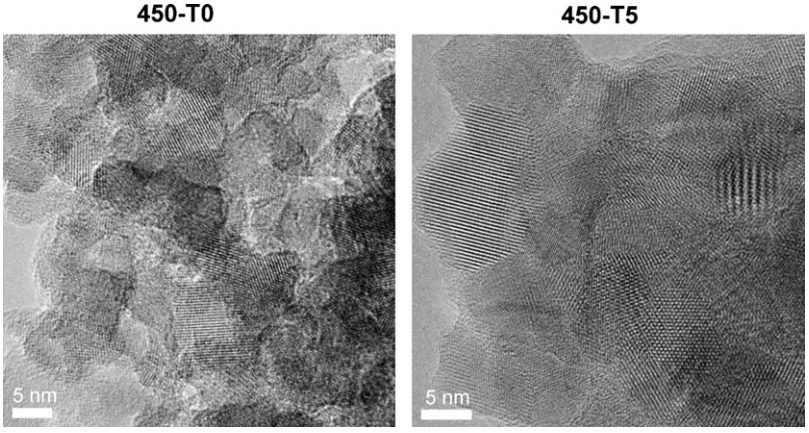

Fig. 2. High resolution TEM pictures representative of the indicated catalysts.

Table 1
Main morphological/structural and surface characteristics of the examined samples.

Sample	Crystal size[a] (nm)	Cell parameters[a] $a=b$, c (Å)	Cell volume[a] (Å^3)	Average particle size[b] (nm)	S_{BET} (m^2 g^{-1})	XPS binding energies (eV) of main peaks		Fe/Ti atomic ratio	
						Ti 2p$_{3/2}$	Fe 2p$_{3/2}$	Surface XPS	Bulk ICP-OES
450-T0	9.9	3.78, 9.48	135.5	9.1	77.6				
450-T1	12.7	3.79, 9.46	135.5		72.0	459.0	711.0	0.0095	0.01
450-T5	10.5	3.79, 9.31	133.6	11.5	96.1	458.5	710.9	0.041	0.05

[a] For the anatase phase of titania, from XRD results.
[b] For primary particles, from high resolution TEM pictures, considering Feret's diameters and volumetric average ($\sum n_i d_i^4 / \sum n_i d_i^3$).

of aggregated oxidic iron entities, in correlation with previous EPR analysis [10]; the important increase observed for the latter in 450-T5 suggests the prevailing presence of such entities in this system. On the other hand, as summarized in Table 1, XPS analysis of main peaks in Ti 2p and Fe 2p zones is consistent with values detected for Ti^{4+} cations in TiO_2 and Fe^{3+} species, respectively [17]. In turn, Fe/Ti atomic ratio values determined for the catalysts calcined at 450 °C are close to bulk ones, in accordance with achievement of a relatively high iron dispersion in such systems; nevertheless, a relatively higher shift with respect to the bulk value is detected for 450-T5, in consistency with proposed presence of a higher amount of segregated iron in the form of aggregated iron oxide entities for such sample [10].

3.2. Photoactivity measurements

Fig. 4 shows the time–evolution curves for phenol and TOC conversions during photocatalytic degradation of phenol with H_2O_2 over the catalysts. Phenol photolysis in the absence of solid catalyst can be considered practically negligible since very slow phenol degradation with practically no change in TOC content was observed in the corresponding blank experiment (not shown). Concerning the influence of iron loading, the catalyst with highest iron content (3.5 wt.%) displays highest phenol photodegradation rates whereas the lowest iron content catalyst (0.7 wt.%) shows relatively poor photodegradation performance, not improving in any case the photocatalytic behaviour of the corresponding undoped catalyst. On the other hand, the evolutions of hydrogen peroxide disappearance along irradiation time fairly follow those of phenol/TOC conversion over any of the catalysts, thus indicating that hydrogen peroxide acts as oxidant in any case and H_2O_2 self-decomposition upon hydroxyl radical scavenging appears limited; it must also be noted in this sense that phenol photodegradation rates are considerably higher than those detected in the absence of hydrogen peroxide (i.e. when only dissolved oxygen from air acts as oxidant) [26]. It can be also noted that comparison between most active 450-T5 catalyst and commercial TiO_2 P25 from Degussa reveals the promising characteristics of this iron-doped catalyst for the solar photodegradation of phenol under pilot plant conditions, since it apparently enhances both phenol and TOC conversion levels with a more efficient handling of the H_2O_2 reactant (considering the similar hydrogen peroxide conversions achieved) for the photodegradation process (Fig. 4).

On the other hand, it can be observed that although complete phenol conversion is always achieved, very little amounts of some intermediate oxidation products still remain at the end of the test, as revealed by residual TOC conversions detected (Fig. 4). Products remaining at the end of the runs correspond to short-chain organic acids, mainly maleic acid, without significance in terms of toxicity. Evolution of all identified oxidation intermediates detected during the course of the runs is presented in Figs. 5 and 6. Firstly, it can be seen that the rates of formation and disappearance of aromatic intermediates was particularly high over 450-T0 and 450-T5 catalysts for which no aromatic organic compound was detected after 40 min. In contrast, long irradiation times were needed for total

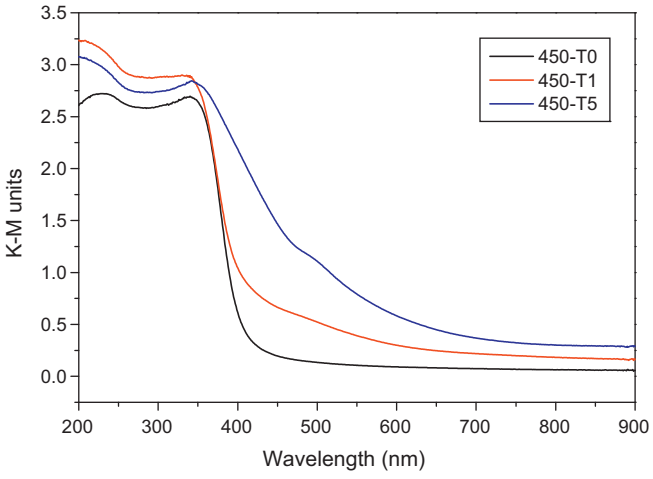

Fig. 3. UV–vis spectra of the indicated catalysts.

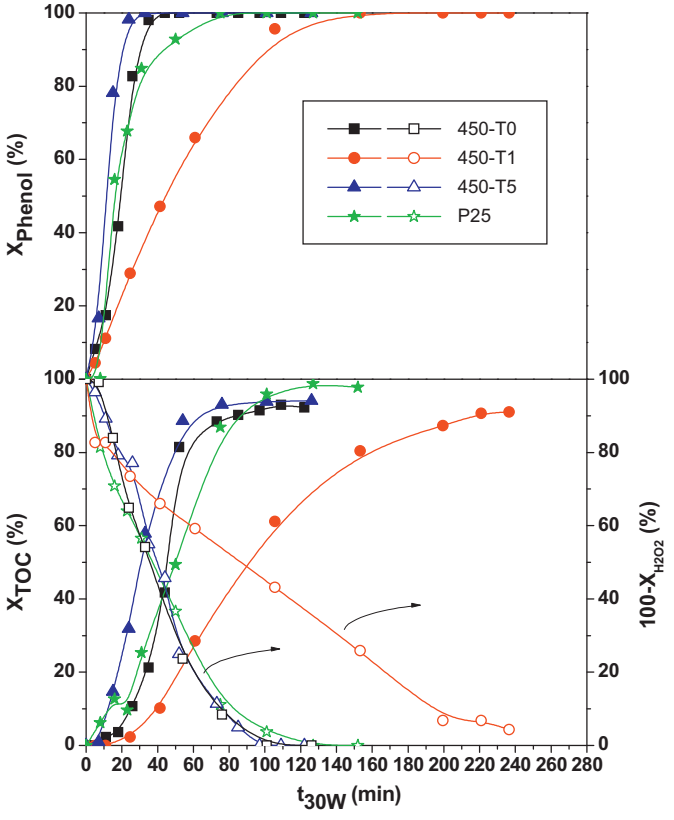

Fig. 4. Evolution of the TOC and phenol conversions (full symbols, solid lines) and hydrogen peroxide reverse conversion (open symbols, dashed lines) during phenol solar photodegradation over the indicated catalysts.

Table 2
Summary of literature results on photodegradation of phenol or related compounds employing series of iron-doped TiO_2 catalysts.

Catalysts characteristics	Reaction conditions	Catalytic activity results and relevant remarks	Ref.
Series of iron-doped titania photocatalysts prepared by sol–gel method with iron content between 0.18 and 7.17 at.%, anatase percentage between 73 and 99% (the rest amorphous TiO_2 or brookite) and anatase crystal size between 15 and 25 nm.	Phenol photooxidation with air and either UV or visible light lamps.	The activity (measured as initial phenol decomposition rate) increases with iron content up to a maximum for the catalyst with 2.24 at.% Fe, either under UV or visible irradiation (2.85 and 4.50 times higher than that shown by the sample with 0.18 at.% Fe, respectively). Correspondence between local structure of Fe(III) and the photocatalytic activity of TiO_2 photocatalysts pointed out, the presence of vacancies for relatively low Fe contents proposed to be beneficial.	[28]
Series of iron-doped titania photocatalysts prepared by flame hydrolysis with iron content between 0.02 and 0.90 at.%, anatase percentage between 68 and 88% (the rest rutile) and anatase crystal size between 44 and 57 nm.	Phenol photooxidation with air and either UV or visible light lamps.	Initial phenol decomposition rate significantly decreases with increasing the iron content either under UV or vis light.	[28]
Series of iron/titania catalysts prepared by impregnation of TiO_2 Degussa P25 between 0 and 1 wt.% Fe and anatase crystal size between 16.4 and 22.3 nm.	4-Nitrophenol photodegradation with O_2 and UV–vis blacklight fluorescent lamps at pH_0 5.9 (natural pH).	The photodegradation percentage or first order rate constant displays a maximum at 0.25 wt.%. Smallest particle size of the sample with such loading pointed out as beneficial.	[29]
Series of iron/titania catalysts prepared by impregnation of anatase TiO_2 (Tioxide-Huntsman) with $S_{BET} = 8\ m^2\ g^{-1}$, iron content between 0 and 8 wt.% and anatase crystal size between 45.9 and 50.5 nm.	4-Nitrophenol photodegradation with H_2O_2 and monochromatic (340 nm) UV lamp at pH_0 6.17 (natural pH) or varying pH (between 3.5 and 8.2).	Maximum photodegradation activity at natural pH is achieved for the photocatalyst with 1 wt.% Fe. Photodegradation rate for such catalyst is shown to increase with decreasing the solution pH.	[30]
Series of iron-doped titania samples prepared by sol–gel method, with 0 to 2.9 mol.% Fe and anatase crystals of 8.3–11.4 nm.	Phenol photodegradation with air and high pressure UV lamp at pH_0 5.	Maximum photoactivity observed for the catalyst with 0.5 mol.% Fe. Above such Fe loading, relatively poor photodegradation efficiency (apparently lower activity than undoped sample) observed.	[31]
Series of iron-doped titania photocatalysts prepared by combined microemulsion/sol–gel method (same catalysts as here) Fe wt.% between 0 and 5.2, S_{BET} between ca. 80 and 120 $m^2\ g^{-1}$ and anatase crystal size between ca. 8 and 13 nm.	Phenol photodegradation with flowing air and high pressure Hg UV lamp at initial pH_0 of 3.0.	Maximum phenol photodegradation activity observed at intermediate 0.7 wt.% Fe content. Achievement of high levels of surface segregation of iron containing amorphous oxidic phases pointed out to explain decrease of photoactivity for higher iron doping levels.	[10]
Series of iron-doped titania photocatalysts prepared by combined microemulsion/sol–gel method (same catalysts as here) Fe wt.% between 0 and 2.9, S_{BET} between ca. 80 and 120 $m^2\ g^{-1}$ and anatase crystal size between ca. 8 and 13 nm.	Phenol photodegradation with flowing air and high pressure Hg UV lamp at initial pH_0 of 6.0.	The phenol photodegradation activity monotonously decreases with increasing the iron content. Samples above 1 wt.% Fe content display very low TOC conversion level.	[32]
Series of iron-doped TiO_2 prepared by combined sol–gel/hydrothermal method, with Fe wt.% content between 0 and 0.9 and anatase crystal size between ca. 11 and 20 nm.	2,4,6-Trichlorophenol photodegradation with air and UV Hg lamps.	Maximum photodegradation achieved for intermediate Fe loading of 0.45 wt.%. Sample with 0.9 wt.% Fe displays lower photoactivity than the undoped sample.	[33]
Series of Fe-doped titanium dioxide anatase microspheres with special core–shell structure, prepared by hydro-alcohol thermal method, with 0–2.0 mol.% Fe content, S_{BET} between 105 and 116 $m^2\ g^{-1}$ and anatase crystal sizes between 8.0 and 11.0 nm.	Phenol photodegradation with air and either UV (fluorescent lamps with maximum at 254 nm) or visible (fluorescent lamps with maximum at 420 nm and 400 nm cut-off filter) light; pH_0 7.	Maximum degradation with UV light for 0.1–0.5 mol.% Fe content; very poor photodegradation activity (much lower than that of undoped samples) with UV light for the sample with 2.0 mol.% Fe. Maximum activity with visible light for the sample with 1.0 mol.% Fe.	[34]
Series of Fe-doped TiO_2 prepared by combined sol–gel/microemulsion, with Fe wt.% content between 0 and 4.1; two final temperatures of calcination under air applied as final step in the preparation: 450 and 600 °C, giving rise to samples with S_{BET} = 78–108 (anatase crystals of ca. 10 nm) and 20–38 (anatase or anatase–rutile for Fe-doped samples with 21–37 nm of anatase crystal size) $m^2\ g^{-1}$, respectively.	Phenol photodegradation with air and solar light at semipilot plant scale (PSA) and natural pH_0.	Highest photoactivity among all explored catalysts observed for the undoped sample calcined at 600 °C. In any case, minimum photoactivity occurs for intermediate Fe contents in any of the two series, which is attributed to increased contributions to the photoactivity from iron lixiviated species, increasing with the iron content of the catalysts.	[26]

Table 2 (*Continued*)

Catalysts characteristics	Reaction conditions	Catalytic activity results and relevant remarks	Ref.
Series of Fe-doped TiO_2 prepared by thermal treatment of Fe–Ti glicolates prepared by solvothermal method. Iron loading between 0 and 1.2 mol.%. S_{BET} = 92 $m^2\ g^{-1}$ for the sample with 0.25 mol.% calcined at 400 °C. Anatase crystal size around 6 nm.	Phenol photodegradation with air and UV 400 W high pressure Hg lamp.	Maximum photoactivity observed for a sample with intermediate iron loading of 0.25 mol.%.	[35]
Series of Fe-doped TiO_2 prepared by coprecipitation from aqueous Ti and Fe chlorides. Iron content between 0 and 7.9 at.%. S_{BET} between 50 and 76 $m^2\ g^{-1}$ with anatase crystal size between ca. 15 and 25 nm.	Phenol photodegradation with air and either UV–vis or visible light.	Maximum activity peaks (measured as initial photodegradation rate) at intermediate iron loadings of 2.24 at.% (UV–vis) or 0.89 at.% (vis).	[36]
Series of Fe-doped TiO_2 prepared by calcination at 550 °C of $Fe_xTi_{1-x}S_2$ mixed sulfides with Fe at.% between 0 and 1 and anatase crystal size between 22 and 36 nm.	Phenol photodegradation with air under UV or visible light. pH_0 between 3.9 and 4.1.	Maximum activity achieved by the specimen with 0.5 at.% Fe under either UV or vis light. Samples above such iron loading display worst activity than the undoped sample under UV. All Fe-containing samples display better activities than the undoped sample when using vis light.	[37]
Series of Fe/TiO_2 samples prepared by wet impregnation of home made TiO_2 (displaying anatase/rutile mixture) with Fe mol.% between 0 and 5 and S_{BET} between 53 and 61 $m^2\ g^{-1}$.	4-Nitrophenol photodegradation with O_2 and UV medium pressure Hg lamp at $pH_0 \approx 4.5$.	The photoactivity monotonously decreases with increasing the iron content of the catalyst.	[38]

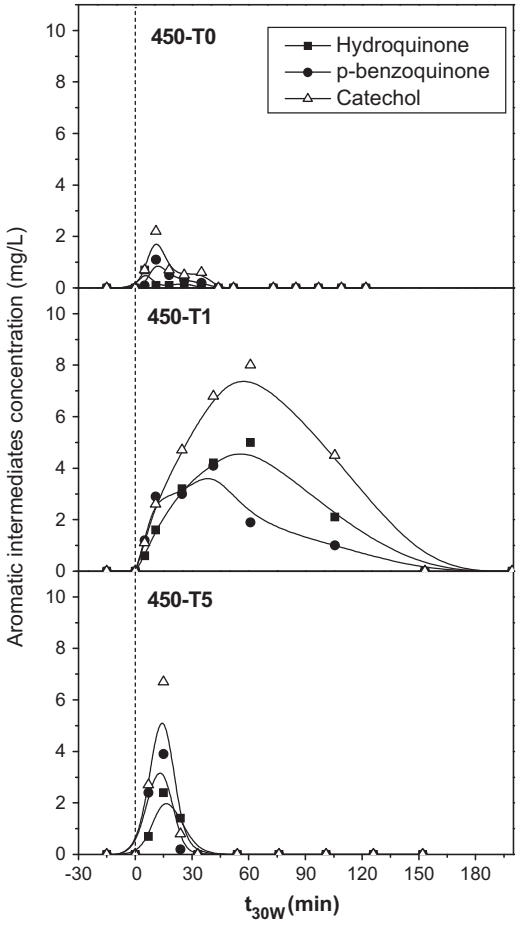

Fig. 5. Evolution of aromatic intermediates formed during the photodegradation of phenol over the indicated catalysts.

aromatic organic matter removal over 450-T1 (Fig. 4), as reflected also by the evolution of organic intermediates (Fig. 5). In any case, catechol, p-benzoquinone and hydroquinone were always the primary oxidation intermediates as result of phenol hydroxylation. The fact that higher catechol concentrations were always observed may be explained as the consequence of a relatively high rate of OH radical generation in the presence of H_2O_2, which contributes to ortho-hydroxilation of the aromatic ring during the photocatalytic process [27]. As an important conclusion, the concentrations of hydroquinone and p-benzoquinone as well as catechol become negligible in all cases after 3 h; it must be considered that these compounds (particularly the two former) are by far the most toxic species during the oxidation route of phenol. Finally, as mentioned, among all short-organic acids detected along the process, maleic acid is fundamentally the main responsible of the slight residual TOC found at the end of the runs (Fig. 6), and therefore the most refractory compound of the photodegradation process [28–38].

In any case, the most intriguing result is the fact that the most active catalyst is, in contrast to typical results (Table 2), that with a relatively high iron loading for which characterization results evidence the presence of, in principle, less active [10,15], surface segregated oxidic iron species. Thus, as collected by Table 2, iron-doped TiO_2 samples generally display either a decrease in the phenol photodegradation rate with increasing the iron amount or a maximum at intermediate iron contents around 1.0 at.% [15], a loading similar to that of 450-T1. Indeed, our previous investigation (on the same catalysts as here studied) employing UV light and oxygen as oxidant at laboratory scale exhibited maximum activity for iron content around 1.0 at.%, at which iron incorporation to the anatase lattice could be maximized (and/or iron segregation, forming less active oxide entities [15], could be minimized [10]), when initial pH was pH_0 3.0 [10]. However, when initial pH was of 6.0 (close to that employed here) while the rest of conditions were the same, highest photoactivity was achieved for the undoped sample and it was shown to decrease monotonously with increasing the amount of iron [32]. The apparent differences as a function of pH certainly indicate the relevancy of surface photoprocesses on overall

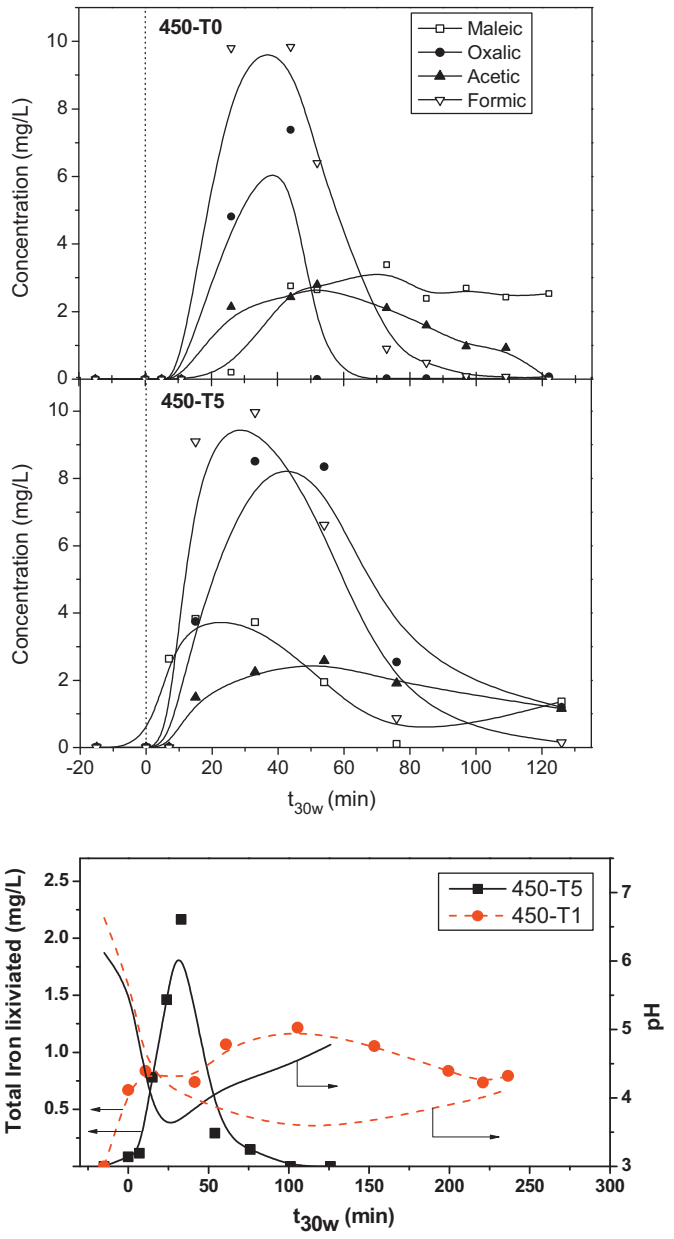

Fig. 6. Top: Evolution of the indicated short chain acids during the course of phenol photodegradation over the indicated catalysts. Bottom: Evolution of total iron lixiviated from the doped catalysts (full symbols) and pH of the solution (lines) during the photodegradation of phenol over 450-T5 (solid lines) and 450-T1 (dashed lines).

photoactivity achieved over this type of catalysts. In any case, the unusually high activity of the sample with highest iron content strongly indicates that new phenomena affecting to the iron component could be taking place during the course of the run and would determine the photoactivity of 450-T5, as discussed in next section.

3.3. Iron leaching from the catalysts

The mentioned particularity can be related to the fact that, as a difference with results obtained under softer conditions employed during experiments with laboratory photoreactors [10], appreciable amounts of iron become lixiviated to the reaction medium (in the form of Fe(II) species according to spectrometric analysis) under the conditions used in these experiments, as illustrated in Fig. 6. It is noted that lixiviated iron evolves in the form of a volcano type curve, particularly in the case of 450-T5 (Fig. 6). This indicates that iron in fact undergoes a leaching/readsorption process, in agreement with the practical absence of changes in the iron contents detected by chemical analysis between initial and used catalysts. It can be also observed that maximum iron lixiviates amount coincide with minimum solution pH values and can be also apparently correlated with observation of maximum concentrations of short-chain organic acids (Fig. 6). Evidence for the iron redistribution as a consequence of the iron lixiviation-readsorption process in 450-T5 has been achieved by UV–vis and XPS spectroscopies (Fig. 7). Thus, the UV–vis spectrum of 450-T5 after reaction reveals a higher absorption at ca. 500 nm which, as mentioned above, has been related to aggregated iron oxide species, thus evidencing the iron segregation induced by the iron lixiviation/readsorption process. In turn, XPS reveals that such iron segregation must be produced at the catalyst surface, as inferred from differences found in Fe/Ti ratio between initial and used catalysts (Fig. 7), giving further support to the mentioned iron reorganization process following leaching and readsorption on the sample surface.

The fact that iron becomes lixiviated to the reaction medium opens the possibility that some contribution from homogeneous photooxidation or related processes (for instance, considering the presence of H_2O_2, photo-Fenton type processes) could take place, particularly for catalysts in which higher amounts of iron lixiviates could be apparently produced, like 450-T5. Alternatively, taking into account that iron becomes readsorbed on the catalyst surface (Fig. 7), the photoactivity could originate from surface adsorbed iron photocomplexes, which are known to enhance the phenol oxidation photoactivity under certain conditions [39]. Indeed, as recently proposed when using oxygen as oxidant [26], iron readsorption on the catalyst surface could result as a consequence of catalytic steps involved in the photodegradation of phenol. On this basis, blank experiments were designed in order to explore these possibilities. Thus, a first experiment consisted in exploring the possibility that homogeneous photo-Fenton could take place and for this purpose the solution of phenol and H_2O_2 was irradiated in the presence of dissolved Fe^{2+}. The second blank test consisted in irradiating the solution of phenol and H_2O_2 with 450-T0 dispersed in it and to which external Fe^{2+} was incorporated to the solution. In any of the cases, concentrations of phenol and H_2O_2 (or 450-T0) were the same as used for the heterogeneous photocatalytic experiments in Fig. 4. In turn, iron was incorporated to the solution or dispersion in four doses of 0.5 mg L^{-1} of Fe^{2+} (to give a total of 2 mg L^{-1}), as specified in Fig. 8, aiming to obtain a situation more similar to that taking place during the heterogeneous photocatalytic test over 450-T5 in which iron must be leached in a progressive way. As shown in Fig. 8, both homogeneous photo-Fenton and addition of external iron to the undoped catalyst enhance the performance of 450-T5, thus disallowing to discriminate between both possibilities on the basis of such experiments alone. In any case, results in Figs. 4–6 show that the new mechanism operates under conditions in which the concentration of iron in the aqueous medium is very low (for instance, close to $t_{30W} = 0$), conditions under which contributions from homogeneous photo-Fenton must be quite limited [40,41], thus suggesting that, as previously proposed when using oxygen as oxidant [26], it must be a mechanism of surface iron photocomplexes which predominates here. On the other hand, it is important to note that such mechanism does not appear to operate in the case of the blank experiment with 450-T0 + Fe^{2+}, in which the iron concentration monotonously increased in the solution in response to increased dosing and then remained at fairly constant concentration throughout the reaction without observing the volcano type curve detected for 450-T5 (Fig. 6). Thus, in summary, considering the correlation between amounts of lixiviated iron and short chain organic acids (Fig. 6), it can be proposed that iron could be extracted from these iron-doped titania catalysts by means of the formation of Fe-carboxylic acid complexes. In this

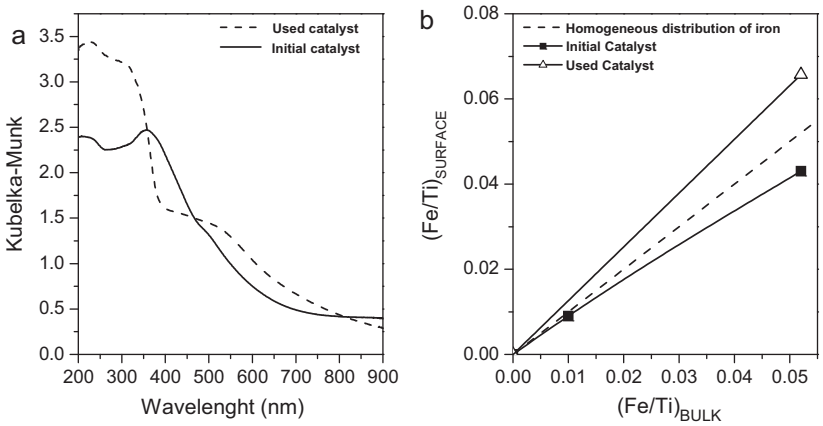

Fig. 7. (a) UV–vis spectra from the catalyst 450-T5 before and after reaction. (b) XPS Fe/Ti atomic ratio for the 450-T5 catalyst before and after reaction.

sense, similar to our case, previous works by Araña et al. and Teoh et al. have shown that short-organic acids can easily extract iron from iron-doped titania catalysts during photooxidation of various carboxylic acids (in particular, maleic, oxalic and formic), after which iron becomes finally readsorbed on the surface of the catalyst [18,19]. As proposed in those works, formation of iron–carboxylic acid complexes can favour the photodecomposition of the organic acid and could be a essential step to explain the high photoactivity detected over 450-T5. On the other hand, readsorption of the iron (Fig. 6) has been attributed to posterior precipitation of Fe^{3+} species formed upon interaction of the decarboxylated Fe^{2+} species with photogenerated holes or oxidized by O_2 [18,26] (or H_2O_2 or oxidant species derived from it), a process which leaves the catalyst ready for the next catalytic cycle. In the case of 450-T1, such mechanism does not appear powerful enough as to contribute significantly to the photoactivity, probably because the amount of iron that could contribute to it is much lower than for 450-T5, prevailing in that case electron–hole recombination processes taking place in the solid, which are unfavourable to its catalytic activity in comparison with the undoped sample [32]. The absence of significant contributions of such mechanism in 450-T1 is in fact reflected by the absence of significant readsorption of the lixiviated iron in such catalyst, taking into account, as mentioned above, that readsorption can take place as a consequence of catalytic steps during phenol photodegradation [26].

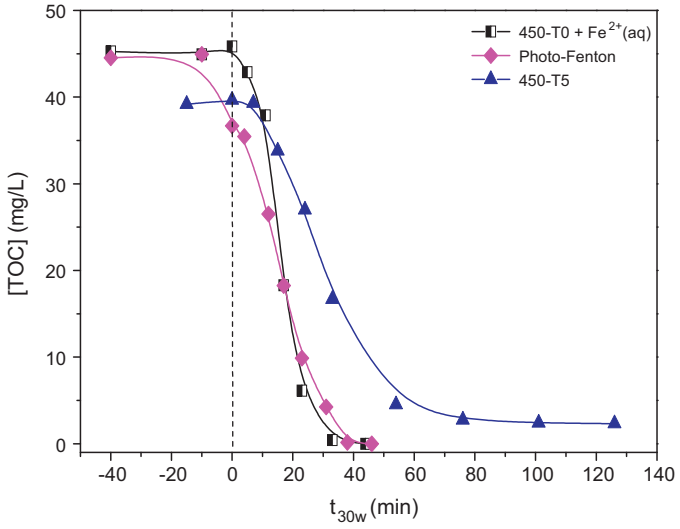

Fig. 8. Evolution of TOC concentration during blank experiments of phenol photodegradation with H_2O_2 including 450-T0 with 2.0 mg L^{-1} Fe^{2+} and photo-Fenton (no solid catalyst) with 2.0 mg L^{-1} Fe^{2+}, in comparison with 450-T5; in any of the two former cases Fe^{2+} was added to the solution in four doses of 0.5 mg L^{-1} of Fe^{2+} at $t_{30W} \approx 0$, 5, 10 and 20 min (see main text for details).

4. Conclusions

By contrast with results generally obtained in the literature and with our previous laboratory experiments, in which optimum photocatalytic properties are achieved either upon doping at a relatively weak level (around 1 wt.%) or the phenol photooxidation activity monotonously decreases with increasing the amount of iron in TiO_2, this study has found that catalysts with a relatively high iron loading display a relatively high phenol photodegradation activity. Such differences could be related with the existence of iron leaching/readsorption phenomena under the employed conditions, which could favour prevailing contributions from homogeneous processes or new photoactive surface complexes to the photoactivity. Correlations found between amounts of lixiviated iron and short chain organic acids detected in the reaction medium, as well as the fact that iron becomes finally readsorbed on the catalyst surface (as evidenced by XPS and UV–vis spectroscopies) suggests a mechanism of solar light-assisted iron carboxylation–decarboxylation process, similar to that proposed recently when using oxygen as oxidant [26]. In turn, it may be noted that the fact that leached iron becomes fully readsorbed on the surface of the catalyst during the course of the reaction opens the interesting possibility from a practical point of view of facilitating separation of the catalyst from reaction products, as a difference with employment of simple homogeneous photo-Fenton.

Acknowledgements

Thanks are due to the MEC (projects CTQ2004-03409/BQU, CTQ2006-15600/BQU and CTM2007-60577/TECNO) and CSIC (project PIF 200420F0280) and Programa de Acceso de Grandes Instalaciones Científicas Españolas GIC-05-17, for financial support. We would also like to thank ICP-CSIC Unidad de Apoyo staff for performing a part of the textural analysis and spectroscopic results, as well as Dr. Laura Pascual for performing the TEM experiments and Prof. J.L.G. Fierro for performing XPS measurements as well as the technical assistance of Agustín Carrión at the PSA.

References

[1] F.J. Beltrán, F.J. Rivas, O. Gimeno, J. Chem. Technol. Biotechnol. 80 (2005) 973.
[2] S. Malato, P. Fernández-Ibáñez, M.I. Maldonado, J. Blanco, W. Gernjak, Catal. Today 147 (2009) 1.

[3] M.A. Shannon, P.W. Bohn, M. Elimelech, J.G. Georgiadis, B.J. Mariñas, A.M. Mayes, Nature 452 (2008) 301.
[4] V. Augugliaro, M. Litter, L. Palmisano, J. Soria, J. Photochem. Photobiol. C 7 (2006) 127.
[5] J.M. Herrmann, Top. Catal. 14 (2005) 49.
[6] D.F. Ollis, E. Pellizetti, N. Serpone, Environ. Sci. Technol. 25 (1991) 1522.
[7] M.R. Hoffmann, S.T. Martin, W. Choi, D. Bahnemann, Chem. Rev. 95 (1995) 69.
[8] M. Anpo, M. Tackeuchi, J. Catal. 216 (2003) 505.
[9] V. Augugliaro, C. Baiocchi, A.B. Prevot, E. García-López, V. Loddo, S. Malato, G. Marcí, L. Palmisano, M. Pazzi, E. Pramauro, Chemosphere 49 (2002) 1223.
[10] C. Adán, A. Bahamonde, M. Fernández-García, A. Martínez-Arias, Appl. Catal. B 72 (2007) 11.
[11] A. Fuerte, M.D. Hernández-Alonso, A.J. Maira, A. Martínez-Arias, M. Fernández-García, J.C. Conesa, J. Soria, Chem. Commun. (2001) 2178.
[12] K.L. Yeung, A.J. Maira, J. Stolz, E. Hung, N.K.C. Hu, A.C. Wei, J. Soria, K.J. Cho, J. Phys. Chem. B 106 (2002) 4608.
[13] A. Kubacka, G. Colón, M. Fernández-García, Catal. Today 143 (2009) 286.
[14] R.I. Bickley, J.S. Lees, R.J.D. Tilley, L. Palmisano, M. Schiavello, J. Chem. Soc. Faraday Trans. 88 (1992) 377.
[15] M. Litter, J.A. Navío, J. Photochem. Photobiol. A 98 (1996) 171.
[16] E. Piera, M.I. Tejedor-Tejedor, M.E. Zorn, M.A. Anderson, Appl. Catal. B 46 (2003) 671.
[17] J. Zhu, F. Chen, J. Zhang, H. Chen, M. Anpo, J. Photochem. Photobiol. A 180 (2006) 196.
[18] J. Araña, O. González Díaz, J.M. Rodríguez, J.A. Herrera Melián, C. Garriga i Cabo, J. Pérez Peña, M.C. Hidalgo, J.A. Navío-Santos, J. Mol. Catal. A 197 (2003) 157.
[19] W.Y. Teoh, R. Amal, L. Mädler, S.E. Pratsinis, Catal. Today 120 (2007) 203.
[20] T.Y. Wei, Y.Y. Wang, C.C. Wan, J. Photochem. Photobiol. A 55 (1990) 115.
[21] B. Tryba, Int. J. Photoenergy, art. n° 721824 (2008).
[22] C.D. Wagner, L.E. Davis, M.V. Zeller, J.A. Taylor, R.H. Raymond, L.H. Gale, Surf. Interface Anal. 3 (1981) 211.
[23] S. Malato, J. Blanco, M.I. Maldonado, P. Fernández, D. Alarcón, M. Collares, J. Farinha, J. Correia, Solar Energy 77 (2004) 513.
[24] M. Hincapié Pérez, G. Peñuela, M.I. Maldonado, O. Malato, P. Fernández-Ibáñez, I. Oller, W. Gernjak, S. Malato, Appl. Catal. B 64 (2006) 272.
[25] H. Zhang, J.F. Banfield, J. Phys. Chem. B 104 (2000) 3481.
[26] C. Adán, A. Martínez-Arias, S. Malato, A. Bahamonde, Appl. Catal. B 93 (2009) 96.
[27] J.A. Zazo, J.A. Casas, A.F. Mohedano, M.A. Gilarranz, J.J. Rodríguez, Environ. Sci. Technol. 39 (2005) 9295.
[28] É.G. Bajnóczi, N. Balázs, K. Mogyorósi, D.F. Srankó, Z. Pap, Z. Ambrus, S.E. Canton, K. Norén, E. Kuzmann, A. Vértes, Z. Homonnay, A. Oszkó, I. Pálinkó, P. Sipo, Appl. Catal. B 103 (2011) 232.
[29] Y. Yalçın, M. Kılıç, Z. Çınar, Appl. Catal. B 99 (2010) 469.
[30] B. Zhao, G. Mele, I. Pio, J. Li, L. Palmisano, G. Vasapollo, J. Hazard. Mater. 176 (2010) 569.
[31] K. Naeem, F. Ouyang, Physica B 405 (2010) 221.
[32] C. Adán, J. Carbajo, A. Bahamonde, A. Martínez-Arias, Catal. Today 143 (2009) 247.
[33] P. Vijayan, C. Suresh, K. Shanthi, Catal. Today 141 (2009) 220.
[34] J. Li, J. Xu, W.-L. Dai, H. Li, K. Fan, Appl. Catal. B 85 (2009) 162.
[35] X.-X. Zou, G.-D. Li, M.-Y. Guo, X.-H. Li, D.-P. Liu, J. Su, J.-S. Chen, Chem. Eur. J. 14 (2008) 11123.
[36] Z. Ambrus, N. Balázs, T. Alapi, G. Wittmann, P. Sipos, A. Dombi, K. Mogyorósi, Appl. Catal. B 81 (2008) 27.
[37] M.S. Nahar, K. Hasegawa, S. Kagaya, Chemosphere 65 (2006) 1976.
[38] A. Di Paola, G. Marcí, L. Palmisano, M. Schiavello, K. Uosaki, S. Ikeda, B. Ohtani, J. Phys. Chem. B 106 (2002) 637.
[39] M.S. Nahar, K. Hasegawa, S. Kagaya, S. Kuroda, J. Hazard. Mater. 162 (2009) 351.
[40] M. Hincapie, M.I. Maldonado, I. Oller, W. Gernjak, J.A. Sánchez-Pérez, M.M. Ballesteros, S. Malato, Catal. Today 101 (2005) 203.
[41] A. Sclafani, L. Palmisano, E. Davi, J. Photochem. Photobiol. A 56 (1991) 113.